Characterizing radiative properties of low and high clouds in different oceanic regions using CERES data

Bing Lin[*1], Patrick Minnis[1], Tai-Fang (Alice) Fan[2],

Yongxiang Hu[1], and Wenbo Sun[3]

[1]Sciences Directorate, NASA Langley Research Center

Hampton, VA 23681

[2]SAIC, One Enterprise Parkway

Hampton, VA 23666

[3]Department of Atmospheric and Planetary Sciences,

Hampton University, Hampton, VA 23668

Submitted to the Journal of Climate

May 2008

[*]Corresponding author's address: Dr. Bing Lin, MS 420, NASA Langley Research Center, Hampton, VA 23681-2199; email: bing.lin@nasa.gov; phone: 757-864-9823; fax: 757-864-7996.

Abstract

Measurements of radiation and cloud properties taken by the Clouds and the Earth's Radiant Energy System (CERES) and Moderate-resolution Imaging Spectroradiometer (MODIS) on the *Aqua* spacecraft are evaluated to determine the similarities and differences in radiation, cloud amount, cloud liquid and ice water paths among the same types of cloud systems. The period from January 2003 to December 2005, unaffected by an El Nino or La Nina, was chosen to establish a set of "normal" conditions for comparisons with models. A total of 13 cloudy marine areas are selected to represent high clouds in the mid-latitude storm tracks and tropical convergence zones and low clouds in the subtropical high-pressure areas dominated by boundary-layer stratus and stratocumulus clouds. The individual measurements of the clouds in these areas are statistically analyzed to take advantage of both gridded and individual cloud system characteristics. Large seasonal and interannual changes in cloud cover are similar for the same types of clouds. The seasonal variations in surface and top-of-atmosphere radiative fluxes for the same types of clouds from different areas are remarkably similar. Although cloud liquid or ice water paths vary considerably for the same types of clouds, their statistical distributions are very stable for different periods and areas. Generally, the seasonal variations of the analyzed clouds are larger than interannual variations. Of all clouds observed, the high clouds from the North Atlantic storm tracks show the greatest variability with the changes in ice water path of about 50 and 10 mg/m^2 seasonally and interannually, respectively. Overall, the results suggest that the regional differences in dynamics and thermodynamics primarily cause changes in the cloud frequency or coverage and only secondarily in the cloud macrophysical characteristics such as ice or liquid water path. Because of this interregional and interannual stability in cloud properties, changes in cloud cover are most likely to have the greatest influence on changes in

the radiation fields, and, hence, climate. This fluctuation in cloud cover or storm frequencies, then, affects the precipitation, atmospheric hydrology, and the overall averages of water amounts of individual cloud types because of extreme high IWP and LWP values of precipitating clouds. These results comprise a set of valuable observations for testing modeled cloud statistics and for improving cloud model parameterizations. Because of the stable statistical characteristics of cloud water amount and radiation, they have great potential for reducing the large uncertainties in modeled cloud radiative forcing.

1. Introduction

During the last 2-3 decades, the parameterization and representation of cloud properties have been a focus of global climate model (GCM) studies. Yet, significant problems remain for characterizing clouds accurately in the models, and subsequently the changes in clouds and their feedbacks with changing climate are highly uncertain. Cloud cover and its vertical distributions determined from GCMs for the current climate differ significantly from the observations despite relatively large uncertainties in the latter [*Zhang et al.*, 2005]. The cloud ice water paths (IWP) derived by GCMs are highly model dependent and differ markedly from the observations in many cases [*Waliser et al.*, 2008]. Some of these problems are caused by theoretical and numerical modeling shortcomings, and the others are due to uncertainties in the observations. Much additional work is needed to better understand the observations and to develop more accurate cloud parameterizations, especially for particular cloud types.

For example, tropical deep convective systems not only generate heavy precipitation and transport moisture to the upper troposphere but also have crucial effects on atmospheric radiation due to their large horizontal and vertical extents. Marine boundary-layer clouds, mostly formed in the subtropical regions, form under the subsidence of the Hadley and Walker circulations and the temperature inversion associated with the top of the boundary layer. Because of the preferred large-scale dynamics and local thermodynamics, marine boundary-layer clouds, in particular stratus and stratocumulus, impose a persistent negative radiative forcing, or cooling, that affects the tropical atmospheric circulation patterns. The radiative properties of these clouds, such as optical depth (τ), liquid water path (LWP), IWP, cloud temperature (Tc), effective cloud droplet radius (Re) and ice crystal diameter (De), shortwave (SW) and longwave (LW) fluxes, and cloud areal coverage (Ac), range from very small to extremely large values. Current cloud

parameterizations in GCMs and, even, in cloud resolving models cannot simulate all of the detailed physical processes that operate inside clouds and within the boundary layer.

Most knowledge of clouds and their feedbacks has been obtained from observations of cloud water amount (or its closely related variable, optical depth), particle size, and associated radiation. Satellite and ground-based measurements revealed that the change in cloud thickness, not adiabatic cloud water content, is the primary cause of the LWP variation with temperature [*Tselioudis et al.* 1992; *Del Genio and Wolf*, 2000; *Lin et al.* 2003]. The base and top heights of low clouds are significantly coupled with boundary-layer moisture, especially the relative humidity. For high clouds, although there were significant differences in the interpretations of satellite observations during the last decade or so [e.g., *Ramanathan and Collins*, 1991; *Fu et al*. 1992; *Hartmann and Michelsen*, 1993, 2002; *Lindzen et al.* 2001], studies based on the latest satellite observations [*Lin et al.* 2002; *Del Genio and Kovari*, 2002; *Del Genio et al*., 2005; Rapp et al. 2005; Su et al. 2006; Lin et al 2006, 2007] appear to be converging. These studies indicate that although the cloud coverage and ice water content of tropical convective systems may increase in response to climate perturbations or sea surface temperature (SST) variations, the absolute change in radiation of the convective systems should be much weaker than that proposed by the iris and thermostat hypotheses.

A typical approach for characterizing large-scale cloud properties is to compute averages of gridded satellite measurements [e.g., *Tselioudis et al.* 1992; *Cess et al.* 2001]. The advantage of this approach is that the observed averages can be directly used to compare with the results from GCMs due to the similarities in climate regimes and large-scale dynamical forcings. Even the grid sizes and temporal resolutions are generally similar. Also, the computational resources and requirements in data processing are normally manageable for most modeling institutes. A

disadvantage is that different types of clouds are likely mixed together in the gridded data, especially for monthly or longer time scale means. The detailed physical properties associated with individual cloud types, thus, may not be obtained. To overcome this problem, another approach that analyzes individual cloud types, systems, and objects is also frequently used for satellite observations. Such approach can trace the back trajectory of individual clouds and evaluate the life cycle of these clouds [*Machado et al.*, 1998; *Luo and Rossow* 2004]. The radiative properties of huge cloud systems and the influence of environmental conditions on these systems can also be specifically identified [*Lin et al.* 2006, 2007]. Furthermore, the statistics that characterize particular cloud objects are observed [*Machado et al.*, 1998; *Xu et al.*, 2005, 2008; *Eitzen et al.*, 2008]. Because of the complexity in identifying individual cloud systems and the satellite data availability, there is generally no long-term (e.g., interannual) statistical analysis in cloud objects [*Xu et al.*, 2005, 2008; *Eitzen et al.*, 2008]. Although this approach targets the statistics and physical processes of cloud systems, GCMs may not be capable of replicating the observations of individual clouds and generally cannot trace individual cloud systems due to spatial scale differences in the observational analysis and model simulations. The computational power requirements for this approach are also very high.

This study takes advantage of both gridded and individual cloud system analyses, and evaluates same types of clouds occurring at different geographical locations. We will evaluate the consistencies and differences in the characteristics of cloud systems for different times and places with the goal of providing modelers with a basic tool for modeling and assessing observed and simulated clouds. The potential analysis regions are first identified from the gridded annual mean satellite data based on clouds belonging to similar climate regimes. Within these identified regions, the statistical characteristics for each cloud type are computed using radiative fluxes

118 from each Clouds and the Earth's Radiant Energy System (CERES; *Wielicki et al.* [1996])
119 scanner pixel and cloud properties derived from matched Moderate-resolution Imaging
120 Spectroradiometer (MODIS) measurements. The next section introduces the data sets and
121 analysis methods, and Section 3 presents the observational results for the different cloud types.
122 The similarity and difference among the clouds from different regions are discussed. Section 4
123 summarizes the findings of this study.
124

125 **2. Data Analysis**

126 The measurements used here were taken by instruments on the *Aqua* satellite from
127 January 2003 through December 2005 when there were no significant global or tropical scale
128 climatological anomalies such as El Nino and La Nina. Thus, our satellite observed results
129 should represent clouds in fairly average climate conditions. This time period is also constrained
130 by the availability of the CERES single scanner footprint (SSF) product that includes the
131 temporally and spatially matched CERES and MODIS measurements.

132 CERES measures top-of-atmosphere (TOA) broadband SW and LW radiances directly at
133 a spatial resolution of about 20 km, and estimates both TOA and surface SW, LW and net
134 radiative fluxes based on the radiance measurements and the merged MODIS-based cloud and
135 aerosol information. By merging the cloud and radiance measurements, CERES is able to reduce
136 the TOA SW and LW radiative fluxes for specific cloud (and clear) types down to instantaneous
137 errors of ~13 and ~4.3 W/m^2, respectively, values at least a factor of two smaller than those from
138 the Earth Radiation Budget Experiment (ERBE; *Barkstrom et al.* [1989]). The errors in averaged
139 values are significantly smaller. For surface radiative fluxes, the estimated error uncertainties in
140 regional monthly means are about 10 W/m^2 [*Lin et al*., 2008].

141 The cloud properties derived by CERES mission are based on the *Aqua* MODIS 1-km
142 visible (VIS; 0.64 μm), infrared (IR; 10.8 μm), solar infrared (3.8 μm) and split-window (12.0
143 μm) measurements after first classifying each pixel as clear or cloudy as discussed in *Minnis et*
144 *al.* [2008]. For the cloudy pixels, the effective cloud temperature and height, cloud
145 thermodynamic phase (P_{wi}), and the other microphysical properties mentioned earlier are
146 retrieved using updates of the VIS-IR-Solar-IR-Split-window technique (VISST) during the day
147 and the Solar-infrared-IR-Split-window technique (SIST) at night [*Minnis et al.*, 1995, 2004].
148 For this study, the retrievals of cloud LWP, IWP and optical depth are only available for daytime
149 MODIS measurements taken near 13:30 local time. Other cloud properties, such as cloud top
150 temperature and pressure, are estimated from both day- and night-time MODIS measurements.
151 After the CERES cloud retrieval for each MODIS pixel, all cloud properties from the MODIS
152 data are convolved into the corresponding CERES footprint, minimizing spatial and temporal
153 collocation errors.

154 These *Aqua* Edition-1 CERES SSF data are used to identify certain cloud types and to
155 select the typical regions where those clouds are most common. Initial comparisons with radar
156 and lidar data indicate that the marine boundary-layer cloud heights retrieved by CERES are, on
157 average, ~0.3 km greater than those derived from lidar measurements taken by the Cloud and
158 Aerosol Lidar [*Sun-Mack et al.*, 2007]. While direct validation of the low-cloud optical
159 properties over ocean has not yet been performed, comparisons with retrievals using surface-
160 based radar and radiometer data over land indicate good agreement between the CERES-MODIS
161 and surface retrievals of Re, τ, and LWP [*Dong et al.*, 2008]. The optical properties for optically
162 thin cirrus clouds are also in good agreement with radar and lidar retrievals of De, τ, and IWP
163 [*Mace et al.*, 2005, *Chiriaco et al.*, 2007], and the magnitude and distribution of IWP are very

close to those derived from the CloudSat cloud radar [*Waliser et al.*, 2008]. However, the top heights of optically thin cirrus are typically underestimated by 1 or 2 km by the CERES-MODIS retrievals, and very thin cirrus clouds, typically with $\tau < 0.3$, are not detected [*Mace et al.*, 2005; *Chiriaco et al.*, 2007; *Sun-Mack et al.*, 2007]. Although the detection and cloud top height estimation of thin cirrus clouds may be significantly improved by applying CO_2 slicing technique to MODIS data [Chang and Li, 2005a], current CERES operational cloud retrieval technique for MODIS and other satellite sensors has not implemented the CO_2 method, which may result in overestimations of cloud amounts of middle level clouds [Chang and Li, 2005b]. To avoid mischaracterization of middle clouds, this study only discusses low and high clouds identified in the CERES cloud product. For this study, low and high clouds are defined as those having cloud top pressure greater than 680 hPa and less than 440 hPa, respectively. These cloud classifications are assigned to a given CERES pixel based on the average SSF cloud top pressure.

To select the low and high cloud regions for this study, the annual distributions of these kinds of clouds are examined first. To minimize background variability effects on the retrievals only oceanic clouds are considered. Figure 1 shows the annual mean high (upper panel) and low (lower panel) cloud cover for 2005 obtained from the CERES SSF product. Corresponding to this figure, some typical high and low cloud areas are highlighted and labeled in Figure 2. All climatologically stormy areas are evident as regions with a large (> 18%) mean fraction of high cloud cover. For example, middle latitude storms are highly concentrated on the Atlantic and Pacific storm tracks (areas labeled 1-4 in the upper panel of Figure 2). Some places within these regions even have annual mean high cloud fractions greater than 30%. The areas with the greatest high cloud cover are the tropical western Pacific (TWP) and eastern India Ocean (i.e., areas 5, 6, 8, 9) with peak values up to ~50%. The 9 high-cloud areas include 4 mid-latitude

187 storm track regions (1 each in the North Atlantic, South Atlantic, North Pacific, and South
188 Pacific), and 5 tropical deep convective regions (eastern Pacific and Atlantic intertropical
189 convergence zones (ITCZ), northern and southern TWP, South Pacific Convergence Zone
190 (SPCZ,) northern and southern tropical Indian Ocean). For low clouds, persistent marine stratus
191 and stratocumulus clouds occurring more than 45% of the time year-round are found in the
192 upwelling oceanic areas west of the southern Africa, Australia, California, and South America
193 (labeled as 1-4 in the lower panel of Figure 2). Because of both large spatial coverage and
194 significant optical thickness, these clouds comprise one of the dominant factors that influence the
195 global radiation budget. Note that the low cloud amounts in Figure 1 are likely smaller than
196 those seen elsewhere because the *Aqua* daytime overpass is near the time of minimum cloudiness
197 in marine stratus areas.

198 To compute the cloud properties within each region, only those 1° × 1° grid boxes having
199 annual mean cloud amounts greater than 18% and 45% were used for high and low clouds,
200 respectively, to ensure some uniformity across regions. Because of large-scale atmospheric
201 waves and the intermittent nature of deep convection, mesoscale convective clouds, frontal
202 systems and even stratus clouds generally do not continuously stay in each grid box. The actual
203 cloud properties analyzed for those 1° × 1° grid boxes were, thus, the statistical values from
204 individual CERES pixels satisfying the low and high cloud definitions mentioned previously,
205 i.e., they were obtained from instantaneous satellite observations for each type of the clouds in
206 the selected grids. This way would ensure that large-scale conditions were favorable for the
207 selected cloud types even in local and short-time scales. To obtain their statistically-stable
208 distributions, these individual cloud properties were cumulated in monthly and longer time
209 scales. The purpose of our multiple scale cloud analysis process is to pick up the areas that have

persistently favorable climate conditions for the analyzed clouds to grow (annual scale), to catch up with seasonal variations in the areas for the clouds (monthly scale), and to determine weather conditions for the clouds to develop at the observational moment and individual location. From this and previous considerations, it can be seen that the high or low cloud characteristics considered here conserve the cloud features over a wide range of scales from individual satellite footprints to cumulative quantities of a typical grid box up to the entire selected climatological area at monthly or longer time scales.

3. Results and Discussion

Figures 3 and 4 show the time series of monthly mean cloud cover during the study period for the selected areas. For the storm track areas (Figure 3, upper panel), mean high cloud cover generally varies from 15 to 35 % occurring more frequently during the hemispheric spring and summer seasons. In the marine stratus regimes, the low cloud amounts (Figure 3, lower panel) are generally high, mostly greater than about 50%. These results are consistent with the surface-based climatology [*Klein and Hartmann*, 1993], showing similar seasonal variations and less stratus west of Australia. The strong annual cycles in the eastern Pacific and southeastern Atlantic areas may be related to large seasonal zonal shifts of subsidence in the eastern subtropical Pacific and Atlantic and their associated ocean upwelling variations. Weaker large-scale forcing off the west coast of Australia than in the other three regions produces generally weaker low-level stability and, hence, less persistent boundary-layer clouds [*Klein and Hartmann*, 1993]. The seasonal variability of cloud cover in the southeastern Atlantic (area 1, black) appears to be comparable to those in the eastern Pacific areas although the cloud cover may be a little less than in the other areas. The minimum stratus coverage occurs around the

beginning of each year regardless of hemisphere, suggesting that the forcing mechanisms differ between the hemispheres.

The tropical high cloud amounts (Figure 4), mainly from mesoscale convective systems [*Lin et al.* 2006], in the northern tropical Indian Ocean along the ITCZ (area 9; upper panel) have a larger annual cycle than those in the southern tropical Indian Ocean (area 6) owing to the contrast between the Indian subcontinent and the sea as well as the Indian monsoon. The high clouds in the ITCZ over the northern TWP (area 8) and SPCZ (area 5) have similar areal coverage, while their annual variabilities are 6 months out of phase due to the seasonal shifts in solar radiation. The cirrus and convective clouds in the tropical eastern Pacific and Atlantic (area 7) ITCZs generally are less frequent than those in the northern TWP and the India Ocean and have smaller seasonal changes in areal coverage. For the ITCZ across the globe (areas 7, 8, and 9 combined; lower panel; hereafter also called ITCZ), the annual cycle of high cloud cover is dominated by the northern TWP and India Ocean, at least, for the "normal" climate years analyzed here. During 2003-2005, the ITCZ has not changed from its normal conditions greatly and no double ITCZs were observed. An El Nino or La Nina climate would significantly shift the TWP convergence zones to the central Pacific and cause huge changes in high cloud cover in the tropical eastern Pacific and Atlantic (area 7) [*Cess et al*. 2001].

The high clouds in the Indian Ocean (areas 6 + 9) appear as frequently as those in the tropical western Pacific (areas 5 + 8) since the areas of both northern tropical western Pacific (area 5) and SPCZ (area 8) extend to the middle Pacific, which reduces the averaged high cloud amounts in the whole regions compared those around maritime continents (c.f., Figures 1 and 2). Furthermore, minimal seasonal changes in high clouds within these deep convection areas are found owing to persistent preferred convergence conditions throughout the analyzed normal

256 years. Although extreme climate events could be good opportunities in testing models, the
257 normal climate conditions characterized here should provide a baseline for parameterizing the
258 clouds in GCMs.

259 Histograms of the bulk ice/liquid water paths for the high and low clouds in the selected
260 areas are shown in Figures 5 and 6, respectively, for June, July and August (JJA, left column)
261 and December, January, and February (DJF, right column) for 2003 (black), 2004 (red), and
262 2005 (green). The numbers listed in these figures are the means (left column) and standard
263 deviations (right column) of the distributions. To properly display the statistically-significant
264 characteristics of IWP and LWP distributions, only water path values less than 300 g/m^2 (or 0.3
265 mm) are plotted. For each type of clouds in a given area, the ice and liquid water amount ranges
266 are extremely broad, from close to zero to well above 5,000 g/m^2 [c.f. *Lin and Rossow*, 1997].
267 The frequencies for precipitating clouds with extreme high ice and liquid water paths above
268 1,000 g/m^2 in individual statistical bins (or intervals) are extreme low and not statistically stable
269 [*Lin and Rossow*, 1997]. Actually, even for IWP or LWP at values close to 300 g/m^2 the
270 frequencies are already near zero as indicated in the figures. Because of their rare occurrence the
271 clouds with these extreme IWP and LWP values contribute little to the radiation forcing and
272 budget of their type of clouds although they may influence atmospheric hydrology and
273 precipitation significantly. Because the currently available CERES-MODIS retrievals for
274 precipitating clouds are limited to optical depths $\leq$ 128 [*Minnis et al.*, 1995], the IWP or LWP
275 values are probably underestimated for extremely thick clouds. The extremely high IWP and
276 LWP values obtained by *Lin and Rossow* [1994, 1997] were estimated from satellite passive
277 microwave measurements that are not available for this study. To avoid misleading the statistics
278 of IWP or LWP values due to extreme cases, the values higher than 1,000 g/m^2 are not included

279 in the mean and standard deviation calculations in current study. Because of dramatic variations
280 (or chaotic characteristics of) in storm systems from rainfall cells to extended stratiform anvils
281 and thin cirrus clouds, the standard deviations of the analyzed high clouds are generally much
282 bigger than their corresponding averages (Figure 5) even without the extremely high IWP and
283 LWP values. The IWP distributions of these storms skew towards small IWP values with peaks
284 around 10 g/m^2. Very high frequencies of high cirrus and cirrostratus clouds dominate the
285 radiation fields of these storm cloud systems. As expected, mid-latitude winter storms contain
286 more ice than those during summer seasons. Generally, mid-latitude storms have larger seasonal
287 variations than the tropical systems. For example, the average IWP values for the North Atlantic
288 storm tracks change from about 37 g/m^2 to around 80 g/m^2 during summer and winter seasons,
289 respectively, while the maximum seasonal IWP differences for tropical high clouds are ~15
290 g/m^2, mostly within 10 g/m^2. The seasonal changes in large-scale dynamics, sea surface
291 temperatures, and atmospheric temperature and humidity structures are much greater in mid-
292 latitudes compared to those in the tropics.

293 For low clouds (Figure 6), the mean values are relatively high and vary from ~55 g/m^2 to
294 70 g/m^2 for all selected areas in both summer and winter seasons. Compared with summer
295 values, the winter LWP means may be slightly greater, likely due to reduced relative humidity in
296 the boundary layer during warm months as reported in previous observations and analyses of low
297 cloud variations with temperature [e.g., *Tselioudis et al.* 1992; *Del Genio and Wolf*, 2000; *Lin et*
298 *al.* 2003]. The LWP distributions for individual areas in a specific season have much higher
299 cumulated probabilities around their peak occurring frequencies and means compared to those of
300 high stormy clouds, which results in relatively smaller standard deviations about 2/3 of their
301 corresponding means.

Of all clouds observed, the inter-annual variabilities of these clouds are much smaller than the seasonal variabilities. The high clouds from the North Atlantic storm tracks show the greatest variability with the changes in ice water path of about 50 and 10 mg/m^2 seasonally and interannually, respectively.

The huge variability of individual cloud systems for all of the analyzed clouds poses a great challenge for cloud modeling. However, Figures 5 and 6 show that the probability distributions of condensed water for a given cloud type change very little from year to year in each selected area. The shapes, means, and standard deviations of the same type of clouds from different areas are also very similar. These results demonstrate that the cloud characteristics may vary drastically from one individual cloud system to another. But the overall characteristics of the same cloud types in normal conditions (in other words, forced by similar large-scale dynamics and thermodynamics) are very stable. It is over monthly or longer temporal scales in certain areas that stable statistics of cloud properties for the same type of clouds are obtained and can be meaningfully simulated by models.

The monthly mean TOA net radiative fluxes for clouds in the storm track and stratus deck regions are shown in Figure 7. These values, for the most part, represent the amount of radiation that is gained or lost in the Earth-atmosphere system below cloud top. The high clouds associated with mid-latitude storms (upper panel) are generally thick and reflect significant amounts of solar radiation. During the winter seasons, when solar radiation at these latitudes is weak, there is little shortwave irradiance passing into the atmosphere through the clouds, and the net radiation, a combination of minimal shortwave heating and considerable longwave cooling, thus, becomes negative. This cooling effect can be very strong and drops to as low as about -100 W/m^2. When the insolation is greatest (or summer months), the shortwave radiation can

penetrate into the atmosphere through non-precipitating parts of the storm systems, providing significant amounts of solar heating to the surface and troposphere. The stormy clouds also block most of the strong longwave radiation emitted to space by the warmer seas during summer. These combined shortwave and longwave effects during warm seasons generally heat the storm track areas, although the magnitude of the heating (> ~120W/m^2) is not as large as that in clear conditions or in marine-stratus areas (c.f. lower panel). There, the radiative fluxes in the stratus deck areas display similar but slightly stronger annual cycles compared to those in the storm tracks owing to the annual solar insolation cycle and the strong seasonal cloud variations (Figure 3). A difference between the subtropical low clouds and storm-track high clouds is that in the stratus regions, the net radiation warms the Earth-atmosphere system all year, primarily in the boundary layer and the sea surface (c.f., discussions of Figure 10 below). This year-round warming is a result of greater insolation during winter in these areas compared to that in the mid-latitudes. Although the averaged net radiation for both the mid-latitude storm system and stratus cloud areas is positive (or heating), the cloud radiative forcing, defined as the net radiation difference between all-sky and clear-sky conditions, is negative. That is, the clouds actually cool the atmosphere relative to clear skies because the amount of solar radiation reflected back to space is much greater in cloudy conditions (not shown).

The TOA net radiation for the high clouds in tropical convergence zones (upper panel of Figure 8) varies much less (~100W/m^2) than that in the subtropics and mid-latitudes primarily because of smaller insolation variations. Small changes in sea surface temperature and the atmospheric temperature and humidity profiles around equatorial regions also minimize the radiation variability. Although tropical convective regions (lower panel), such as the Indian Ocean (red), TWP (green), and ITCZ (black) have even less seasonal variability than individual

convection areas, the double peaks of the radiation fields in each annual cycle can be found clearly, especially for those in the ITCZ. Even though cold deep convective systems dominate tropical reflection of shortwave energy and release very little thermal radiation to space, more than half of the solar radiation still manages to enter the troposphere [*Lin et al.*, 2002, 2006]. Thus, the semi-annual equator crossing of the sun leaves a significant signature in the observed radiation records of the high clouds along ITCZ areas.

To further evaluate the similarities and differences of cloud radiation among the same types of clouds from different areas, we artificially shift the TOA net radiation forward 6 months periodically for clouds in the Northern Hemisphere. Figure 9 reveals very consistent annual variations in both the phase and amplitude (250 - 300 W/m^2) of the monthly mean net radiative fluxes from all of the different storm track areas (upper panel) and from all of the stratus regions (lower panel). Even though there are some latitudinal differences (i.e., difference in insolation) among them, the overlap of the averaged radiative fluxes for the analyzed storm track regions is so tight that it confirms certain inherit cloud-type features, such as similar ice water amount and variability of these clouds (c.f. Figure 5). As mentioned previously, although extreme precipitating clouds are important for upper-tropospheric moisture transport, cirrus and anvil formation, and climate hydrology [*Lin et al.* 2006] and may not have a stable statistic in an area for an individual month, such clouds are so rare that they do not significantly alter the basic radiative statistics for this cloud type. It is the normal clouds that dominate the radiation statistics because of their large spatial extent (and/or high frequency).

Compared to the mid-latitude storm clouds, the stratus cloud decks (Figure 9, lower panel) generally have similar annual oscillations in their net radiation averages, although these averages (or the net radiative energy into the atmosphere is) are higher because the solar

371 insolation is stronger for these lower latitude clouds. The area off Australia's west coast shows
372 the biggest annual changes in the net radiative fluxes (red) into the Earth's climate system among
373 the four selected stratus deck areas. The largest annual amplitude for the clouds in the area
374 probably is caused by having the highest LWP contrasts between the winter and summer seasons
375 (the differences slightly exceed 10 g/m^2; c.f. Figure 6).

376 Overall, for all of the cloud types, the inter-hemispheric radiation differences between
377 clouds from northern and southern hemispheres are minimal (c.f. Figures 8 and 9). It seems that
378 the differences in dynamics and thermodynamics among the various regions and cloud types
379 have significant impacts on the seasonal changes in cloud cover, but appear to affect cloud water
380 content and, hence, radiation only secondarily. From a climate perspective, then, cloud cover is
381 the component that will most affect or be affected by changes in the climate system. That is,
382 changes in the radiation fields will depend mostly on changes in cloud amount in a given region
383 for a particular cloud type. This result, along with the observed IWP and LWP values of these
384 types of clouds (c.f. Figures 5 and 6), provides not only an effective tool for models to test their
385 cloud simulation schemes but also strong evidence for GCM and cloud resolving models to treat
386 same kinds of clouds (i.e., the storms or status clouds in the selected areas) in the same ways
387 even for different times, places and hemispheres.

388 The time series of the surface net radiation for the selected typical areas (Figure 10) have
389 similar seasonal and interannual patterns as those at TOA except with greater magnitudes. The
390 larger positive heating at the surface compared to that at TOA is an indicator of the greenhouse
391 effect of the atmosphere and these clouds. The hemispherically normalized seasonal surface
392 radiation values from different storm track regions (Figure 10, upper panel) follow each other
393 closely reflecting the similarities in shortwave reflection at the TOA and surface, sea surface

394 temperature, and boundary-layer temperature and humidity. Slightly lower net surface radiation
395 for the clouds off the west coast of Australia during winter months compared to those of other
396 stratus deck areas (Figure 10, lower panel) may result from its higher LWP values (c.f. Figure 6).
397 The surface radiation in the ITCZ and SPCZ regions (Figure 11) has almost the same features as
398 those seen for the other cloud types and at the TOA except with much smaller variability. The
399 double peaks in the surface radiation time series for each annual cycle can still be seen in this
400 figure although they are not as pronounced as those of the TOA net radiation fluxes. Very small
401 variations in surface temperature as well as the thermal and moisture structures of the tropical
402 atmosphere with annual cycle reduce interseasonal surface radiation changes, especially for
403 longwave.

404 Time series of the monthly mean IWP and LWP, including extreme values during studied
405 periods, are shown in Figures 12 and 13 for the selected high and low cloud areas, respectively.
406 Because of extreme high IWP and LWP values in very few precipitating clouds [Lin and Rossow,
407 1994, 1997], the overall means are slightly higher than the values shown in the histogram plots
408 (c.f. Figures. 5 and 6), especially for storm-track cases. For low clouds, the differences are small
409 due to infrequent occurrences of extreme precipitation in this type of regime. The averaged
410 retrieved IWP values (about 0.08 mm or 80 g/m^2) in the storm tracks (Figure 12, top panel) are
411 generally higher than those (about 0.05 mm) in tropical convergence zones (Figure 12, middle
412 and bottom panels) due to more thin cirrus clouds in tropical convective systems than in the mid-
413 latitude storms. The current satellite mean IWP retrievals generally agree very well with
414 previous IWP estimates obtained from combined satellite visible, infrared and microwave
415 measurements when the uncertainties in the previous estimates are considered [*Lin and Rossow*
416 1994, 1996]. As noted earlier, they also agree well with those determined from the CloudSat

417 cloud radar [*Waliser et al.*, 2008]. The IWP values for the North Pacific storm track (upper
418 panel, green curve) have the largest seasonal cycles varying from 0.13 mm during winter months
419 to 0.06 mm in summer months. The IWP over the North Atlantic storm track is noisier than its
420 North Pacific counterpart. These small time scale variations may also cause a larger interannual
421 change compared to those in other storm track areas and tropical convergence zones (also c.f.,
422 Figure 5). As mentioned previously, the IWP estimates for tropical high clouds vary minimally
423 during these 3 normal years, especially for the combined tropical and ITCZ regions (Figure 12,
424 bottom panel).

425 The LWP values for the stratus clouds from different areas (Figure 13) are around 0.06
426 mm and exhibit similar seasonal and interannual variations, as shown in the analysis of the
427 histograms in Figure 6. These CERES *Aqua* LWP retrievals are very consistent with our
428 previous combined satellite visible, infrared and microwave measurements [*Lin and Rossow*
429 1994, 1996; *Lin et al*. 1998; *Ho et al.* 2003], suggesting that the techniques for satellite LWP
430 retrievals are generally mature enough for operational or long-term cloud monitoring.

431

432 **4. Summary and Conclusions**

433 This study uses the satellite visible and infrared narrow- and broad-band measurements of
434 the CERES and MODIS instruments on *Aqua* to evaluate the similarities in and differences of
435 cloud radiation and liquid and ice water paths among the same types of clouds. Typical high
436 clouds such as those found in the mid-latitude storm tracks and tropical convergence zones are
437 considered. The subtropical stratus cloud deck areas off the west coasts of major continents were
438 selected to represent low clouds. Generally, the same types of clouds from different areas
439 exhibit significantly different time series of radiative fluxes due mainly to the differences in solar

insolation and local atmospheric profiles. When these clouds are analyzed by accounting for the inter-hemispherical seasonal differences, the discrepancies in the radiative fluxes are remarkably diminished. As expected, the variabilities of individual storms and solid stratus cloud decks are significant: the standard deviations of LWP and IWP values are generally comparable to or even larger than the means for these cloud systems. Although the LWP or IWP distributions of these clouds can exceed the retrieval upper limits, the occurrence frequencies of these extreme satellite pixels are rare. The statistical distributions of water amounts at normal range (0 ~ 1000 g/m^2) are very stable for different periods and areas. These results comprise a set of valuable observations for testing modeled cloud statistics and for improving cloud model parameterizations. Because of the stable statistical characteristics of cloud water amount and radiation, there is great potential for reducing the large uncertainties in modeled cloud radiative forcing. Future work will focus on the investigation of other cloud types such as marine cumulus, polar clouds, and clouds over land areas and on the influence of these clouds on the atmospheric hydrological cycle.

Acknowledgement. The authors would like to express their appreciation to B. Wielicki, G. Gibson, K.-M. Xu, D. Young, and D. Garber for their invaluable comments and suggestions. This research was supported by NASA's CERES mission and the NASA Energy and Water cycle Studies (NEWS) program. The CERES products were obtained from the NASA Langley Atmospheric Sciences Data Center in Hampton, Virginia.

461 **References**

462 Barkstrom, B., et al., The Earth Radiation Budget Experiment (ERBE) archival and April 1985
463 results, Bull. Am. Meteorol. Soc., 70, 1254-1262, 1989.

464 Cess, R., M. Zhang, B. Wielicki, D. Young, X.-L. Zhou, and Y. Nikitenko, The influence of the
465 1998 El Niño upon cloud-radiative forcing over the Pacific warm pool. J. Climate, 14**,** 2129-
466 2137, 2001.

467 Chang, F.-L., and Z. Li, A new method for detection of cirrus-overlapping-water clouds and
468 determination of their optical properties, *J. Atmos. Sci*., 62, 3993-4009, 2005a.

469 Chang, F.-L., and Z. Li, A near-global climatology of single-layer and overlapped clouds and
470 their optical properties retrieved from Terra/MODIS data using a new algorithm, *J. Climate*,
471 18, 4752-4771, 2005b.

472 Chiriaco, M., and co-authors (2007), Comparison of CALIPSO-like, LaRC, and MODIS
473 retrievals of ice cloud properties over SIRTA in France and Florida during CRYSTAL-FACE,
474 *J. Appl. Meteorol. Climatol.*, *46*, 249-272.

475 Del Genio, A., and A. Wolf, Climatic implications of the observed temperature dependence of
476 the liquid water path of low clouds in the southern great plains, J. Climate, 13, 3465-3486,
477 2000.

478 Del Genio, A.D., and W. Kovari, Climatic properties of tropical precipitating convection under
479 varying environmental conditions, J. Clim., 15, 2597-2615, 2002.

480 Del Genio, A.D., W. Kovari, M.-S. Yao, and J. Jonas, Cumulus microphysics and climate
481 sensitivity, J. Clim., 18, 2376-2387, 2005.

Dong, X., P. Minnis, B. Xi, S. Sun-Mack, and Y. Chen (2008), Comparison of CERES-MODIS stratus cloud properties with ground-based measurements at the DOE ARM Southern Great Plains site, *J. Geophys. Res.*, *113*, D03204, doi:10.1029/2007JD008438.

Eitzen, Z., K.-M. Xu, and T. Wong, Statistical Analyses of Satellite Cloud Object Data from CERES. Part V: Relationships Between Physical Properties of Boundary-layer Clouds, J. Climate, 2008 (in press).

Hartmann, D.L., and M.L. Michelson, Large-scale effects on the regulation of tropical sea surface temperature, J. Climate, 6, 2049-2062, 1993.

Hartmann, D. L., and M. L. Michelsen, 2002: No evidence for iris, *Bull. Amer. Meteor. Soc*., 83, 249-254.

Ho, S.-P., B. Lin, P. Minnis, and T.-F. Fan, 2003: Estimation of cloud vertical structure and water amount over tropical oceans using VIRS and TMI data, J. Geophys. Res., 108 (D14), 4419, doi:10.1029/2002JD003298.

Klein, S. A. and D. L. Hartmann, 1993: The seasonal cycle of low stratiform clouds, *J. Climate*, 6, 1587-1606.

Lin, B., and W.B. Rossow, Observations of cloud liquid water path over oceans: Optical and microwave remote sensing methods, *J. Geophys. Res*., 99, 20907-20927, 1994.

Lin, B., and W.B. Rossow, 1996: Seasonal variation of liquid and ice water path in non-precipitating clouds over oceans, *J. Climate*, **9**, 2890-2902.

Lin, B., and W. B. Rossow, 1997: Precipitation water path and rainfall rate estimates over oceans using Special Sensor Microwave Imager and International Satellite Cloud Climatology Project data, *J. Geophys. Res*., 102, 9359-9374.

504 Lin, B., B. Wielicki, P. Minnis, and W.B. Rossow, 1998a: Estimation of water cloud properties
505 from satellite microwave, infrared, and visible measurements in oceanic environments. I:
506 Microwave brightness temperature simulations, J. Geophys. Res., 103, 3873-3886.
507 Lin, B., P. Minnis, B. Wielicki, D.R. Doelling, R. Palikonda, D.F. Young, and T. Uttal, 1998b:
508 Estimation of water cloud properties from satellite microwave, infrared, and visible
509 measurements in oceanic environments. II: Results, J. Geophys. Res., 103, 3887-3905.
510 Lin, B., B. Wielicki, L. Chambers, Y. Hu, and K.-M. Xu, The Iris hypothesis: A negative or
511 positive cloud feedback? *J. Climate*, *15*, 3-7, 2002.
512 Lin, B., P. Minnis, and A. Fan, Cloud liquid water amount variations with temperature observed
513 during SHEBA experiment, *J. Geophys. Res.*, *108* (D14), 4427, doi:10.1029/2002JD002851,
514 2003.
515 Lin, B., B.A. Wielicki, P. Minnis, L. Chambers, K.-M. Xu, Y. Hu, and A. Fan, The effect of
516 environmental conditions on tropical deep convective systems observed from the TRMM
517 satellite, *J. Climate*, *19*, 5745-5761, 2006.
518 Lin, B., K.-M. Xu, P. Minnis, B.A. Wielicki, Y. Hu, L. Chambers, T.F. Fan, and W. Sun,
519 Coincident occurrences of tropical individual cirrus clouds and deep convective systems
520 derived from TRMM observations, *Geophys. Res. Letter*, *34*, L14804,
521 doi:10.1029/2007GL029768, 2007.
522 Lin, B., P.W. Stackhouse Jr., P. Minnis, B.A. Wielicki, Y. Hu, W. Sun, T.-F. Fan, and L.M.
523 Hinkelman, Assessment of global annual atmospheric energy balance from satellite
524 observations, *J. Geophys. Res*., 2008 (in press).
525 Lindzen, R.S., M.-D. Chou, and A. Hou, 2001: Does the Earth have an adaptive infrared iris?
526 *Bull. Amer. Meteor. Soc*., **82**, 417-432.

527 Luo, Z. and W. Rossow, Characterizing tropical cirrus life cycle, evolution, and interaction with
528 upper-tropospheric water vapor using Lagrangian trajectory analysis of satellite observations,
529 *J. Climate*, *17*, 4541-4563, 2004.
530 Luo, Y., K.-M. Xu, B. A. Wielicki, T. Wong, and Z. A. Eitzen, Statistical analyses of satellite
531 cloud object data from CERES. Part III: Comparison with cloud-resolving model simulations
532 of tropical convective clouds. *J. Atmos. Sci.,* **64,** 762-785, 2007.
533 Mace, G. G., Y. Zhang, S. Platnick, M. D. King, P. Minnis, and P. Yang (2005), Evaluation of
534 cirrus cloud properties from MODIS radiances using cloud properties derived from ground-
535 based data collected at the ARM SGP site, *J. Appl. Meteorol.*, *44*, 221-240.
536 Machado, L., W. Rossow, R. Guedes, and A. Walker, Life cycle variations of mesoscale
537 convective systems over Americas, Mon. Wea. Rev., **126**, 1630-1654, 1998.
538 Minnis, P., and co-authors (1995), Cloud Optical Property Retrieval (Subsystem 4.3). "Clouds
539 and the Earth's Radiant Energy System (CERES) Algorithm Theoretical Basis Document,
540 Volume III: Cloud Analyses and Radiance Inversions (Subsystem 4)", *NASA RP 1376 Vol. 3*,
541 pp. 135-176.
542 Minnis, P., and co-authors (2004), Diurnal, seasonal, and interannual variations of cloud
543 properties derived for CERES from imager data, *Proc. 13th AMS Conf. Satellite Oceanogr.*
544 *and Meteorol*., Norfolk, VA, Sept. 20-24, CD-ROM, P6.10.
545 Minnis, P., and co-authors (2007), Ice cloud properties in ice-over-water cloud systems using
546 TRMM VIRS and TMI data, *J. Geophys. Res.*, *112*, D06206, doi:10.1029/2006JD007626.
547 Minnis, P., and co-authors (2008), Cloud detection in non-polar regions for CERES using
548 TRMM VIRS and Terra and Aqua MODIS data, *IEEE Trans. Geosci. Remote Sens.*,
549 Submitted.

550 Ramanathan, V., and W. Collins, 1991: Thermodynamic regulation of ocean warming by cirrus
551 clouds deduced from observations of the 1987 El Nino, Nature, 351, 27-32.
552 Rapp, A., C. Kummerow, W. Berg, and B. Griffith, An evaluation of the proposed mechanism of
553 the adaptive infrared iris hypothesis using TRMM VIRS and PR measurements, J. Climate,
554 18, 4185-4194, 2005.
555 Reynolds, R.W., and T.M. Smith, Improved global sea surface temperature analysis, J. Climate,
556 7, 929-948, 1994.
557 Su, H., W. G. Read, J. H. Jiang, J. W. Waters, D. L. Wu, E. J. Fetzer, Enhanced positive water
558 vapor feedback associated with tropical deep convection: New evidence from Aura MLS,
559 *Geophys. Res. Lett.*, *33*, L05709, doi:10.1029/2005GL025505, 2006.
560 Sun-Mack, S., and coauthors, Integrated cloud-aerosol-radiation product using CERES, MODIS,
561 CALIPSO and CloudSat Data, SPIE Remote Sensing of Clouds and the Atmosphere XII,
562 Proc. of SPIE, Vol. 6745, edited by A. Comerón; R.H. Picard; K. Schäfer; J.R. Slusser; A.
563 Amodeo, paper ID: 674513, 17-19 September 2007, Florence, Italy, 2007.
564 Tselioudis, G., D. Rind, and W. Rossow, Global patterns of cloud optical thickness variation
565 with temperature, J. Climate, **5**, 1642-1657, 1992.
566 Waliser, D., F. Li, C. Woods, J. Bacmeister, J. Chern, A. DelGenio, J. Jiang, M. Kharitondov, Z.
567 Kuang, H. Meng, P. Minnis, S. Platnick, W. B. Rossow, G. Stephens, S. Sun-Mack, W. K.
568 Tao, A. Tompkins, D. Vane, C. Walker, and D. Wu, 2008: Cloud ice: A climate model
569 challenge with signs and expectations of progress. Submitted to *J. Geophys. Res.*
570 Wielicki, B.A., B. Barkstrom, E.F. Harrison, R. Lee, G. Smith, and J. Cooper, Clouds and the
571 Earth's Radiant Energy System (CERES): An Earth observing system experiment, Bull. Am.
572 Meteorol. Soc., 77, 853-868, 1996.

573 Xu, K.-M., T. Wong, B. A. Wielicki, L. Parker, and Z. A. Eitzen, Statistical analyses of cloud
574 object data from CERES. Part I: Methodology and preliminary results of the 1998 El
575 Niño/2000 La Niña. *J. Climate,* **18,** 2497-2514, 2005.
576 Xu, K.-M., T. Wong, B. A. Wielicki, L. Parker, B. Lin, Z. A. Eitzen, and M. Branson, Statistical
577 analyses of satellite cloud object data from CERES. Part II: Tropical convective cloud objects
578 during 1998 El Niño and evidence for supporting the fixed anvil temperature hypothesis. *J.*
579 *Climate,* **20,** 819-842, 2007.
580 Xu, K.-M., T. Wong, B. A. Wielicki, and L. Parker, Statistical analyses of satellite cloud object
581 data from CERES. Part IV: Boundary-layer cloud objects during 1998 El Niño. *J. Climate*,
582 2008 (in press).
583 Zhang, M. H., and co-authors (2005), Comparing clouds and their seasonal variations in 10
584 atmospheric general circulation models with satellite measurements. *J. Geophys. Res.*, **110**,
585 10.1029/2004JD005021.
586

586 **Figure captions**

587 Figure 1. Annual mean high (upper panel) and low (lower panel) cloud distributions from the
588 CERES-MODIS cloud analysis.

589 Figure 2. Selected regions for stormy (upper panel) and stratus (lower panel) clouds. Individual
590 colors and/or numerical labels represent individual cloud areas.

591 Figure 3. Time series of cloud cover (%) for storm track (upper) and stratus (lower) areas.
592 Hereafter, all area numbers or labels indicated in the figures are consistent with those shown
593 in Figure 2 and discussed in the text.

594 Figure 4. Similar as Figure 3, except for selected tropical areas (upper) and combined regions
595 (lower).

596 Figure 5a. Histogram of IWP for high clouds in middle latitude storm tracks during June, July
597 and August (JJA, left) and December, January, and February (DJF, right) for 2003 (black),
598 2004 (red), and 2005 (green). Means and standard deviations are listed in the left and right
599 columns, respectively, in each plot.

600 Figure. 5b. Same as 5a, except for ITCZ areas.

601 Figure 6. Histogram of LWP for stratus clouds during June, July and August (JJA, left) and
602 December, January, and February (DJF, right) for 2003 (black), 2004 (red), and 2005 (green).

603 Figure 7. Time series of TOA monthly mean net radiation (W/m^2) for clouds in storm track
604 (upper), and stratus (lower) areas.

605 Figure 8. Same as Figure 7, except for tropical convergence zones (upper) and their combined
606 high cloud regions (lower).

607 Figure 9. TOA monthly mean net radiation (W/m^2) for clouds in storm track (upper) and stratus
608 (lower) areas. The Northern Hemisphere radiative fluxes are shifted forward 6 months to
609 obtain the fluxes in the same seasons for all selected areas.
610 Figure 10. Same as Figure 9, except for surface (SFC) net radiation.
611 Figure 11. Same as Figure 8, except for surface (SFC) net radiation.
612 Figure 12. Time series of monthly mean IWP (mm) for high clouds in selected areas.
613 Figure 13. Time series of monthly mean LWP (mm) for low clouds in subtropical solid deck
614 areas.
615

615 Figure 1. Annual mean high (upper panel) and low (lower panel) cloud distributions from the

616 CERES-MODIS cloud analysis.

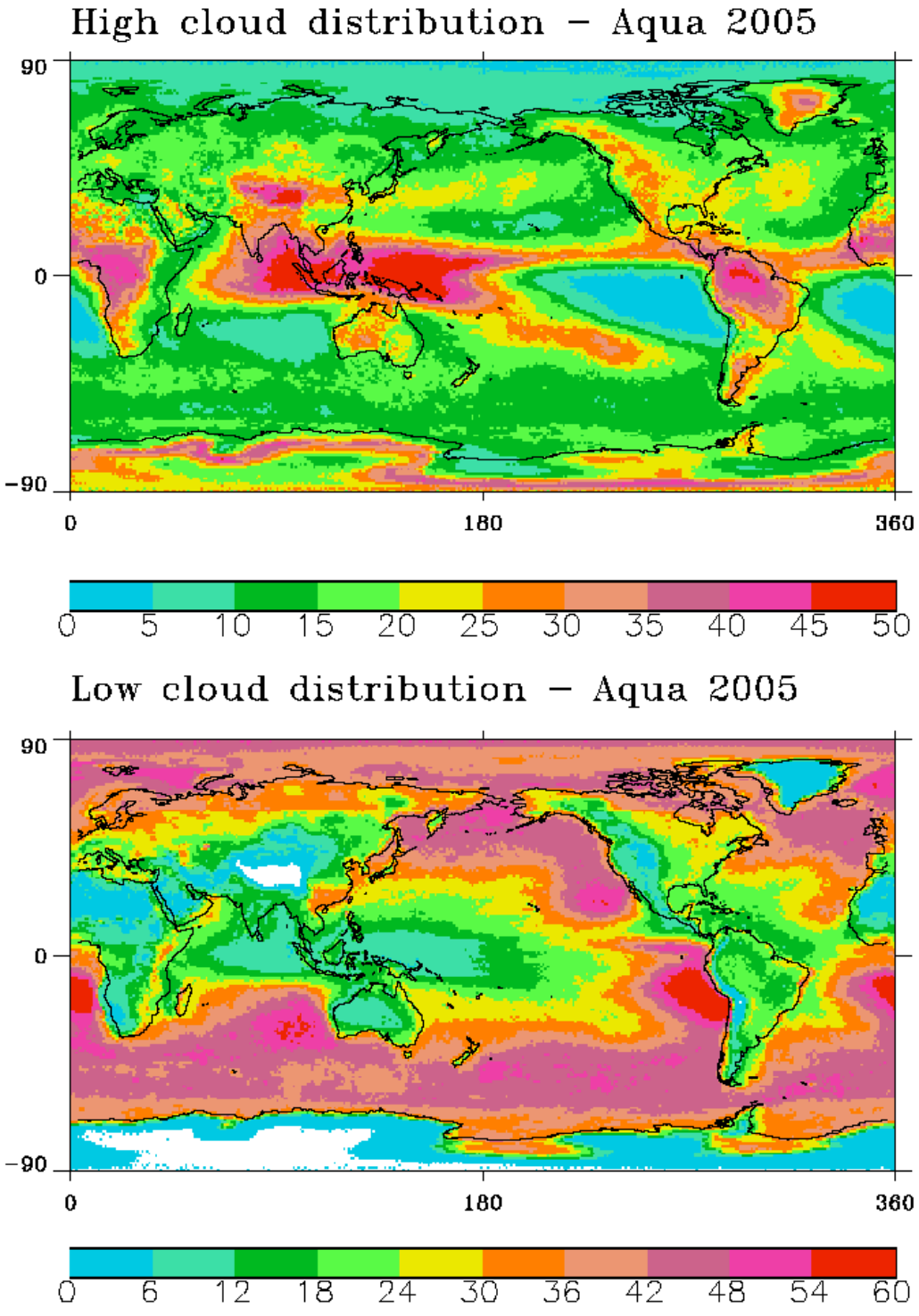

617

618

618 Figure 2. Selected regions for stormy (upper panel) and stratus (lower panel) clouds. Individual
619 colors and/or numerical labels represent individual cloud areas.

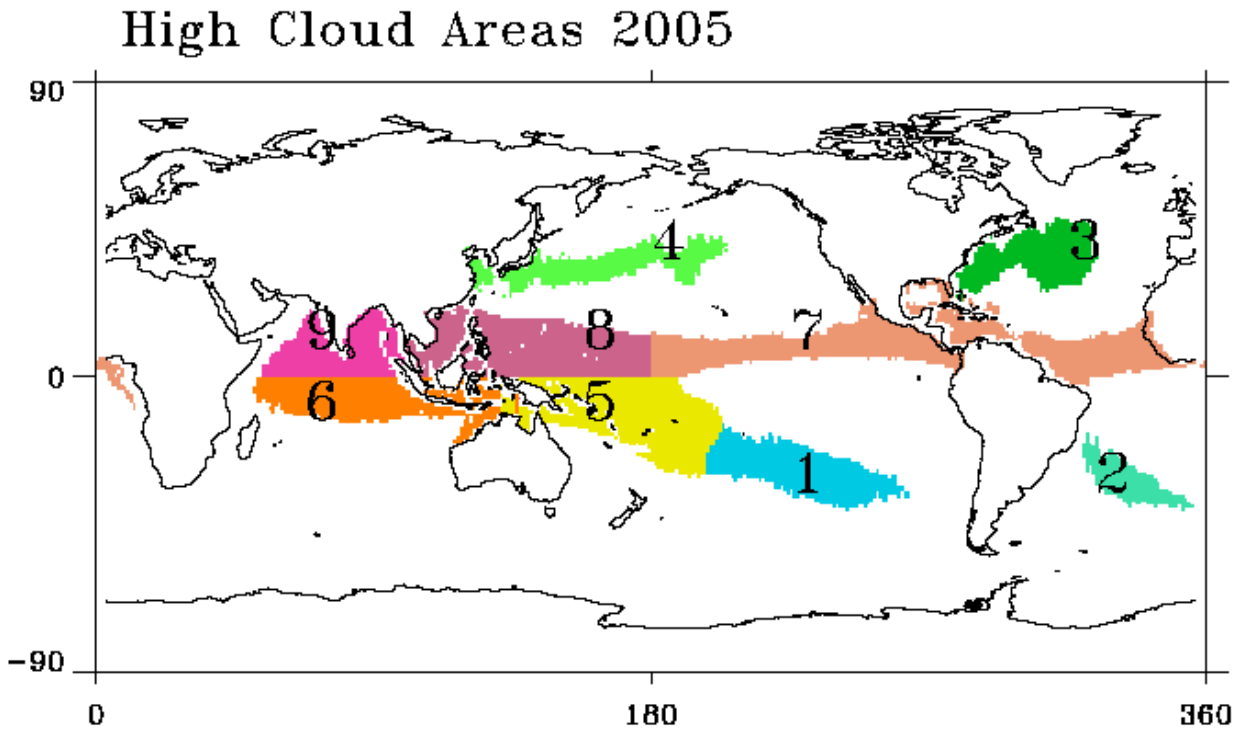

620

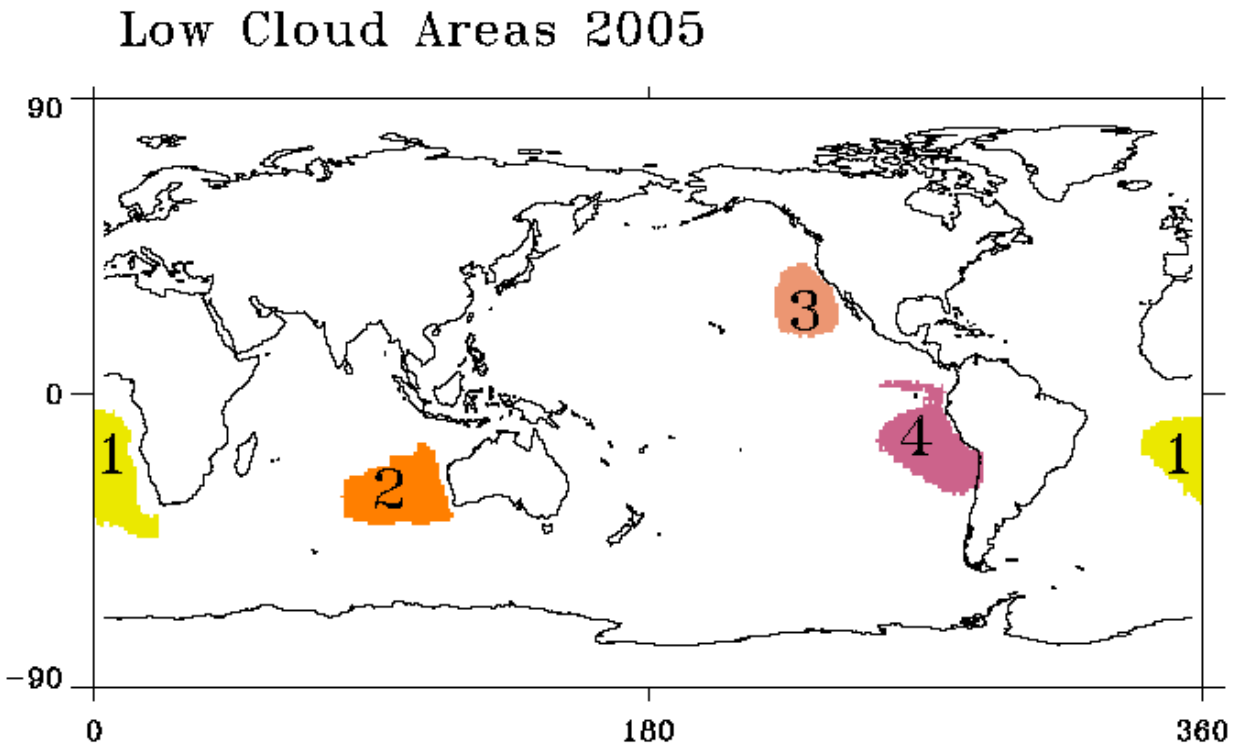

621

622

Figure 3. Time series of cloud cover (%) for storm track (upper) and stratus (lower) areas. Hereafter, all area numbers or labels indicated in the figures are consistent with those shown in Figure 2 and discussed in the text.

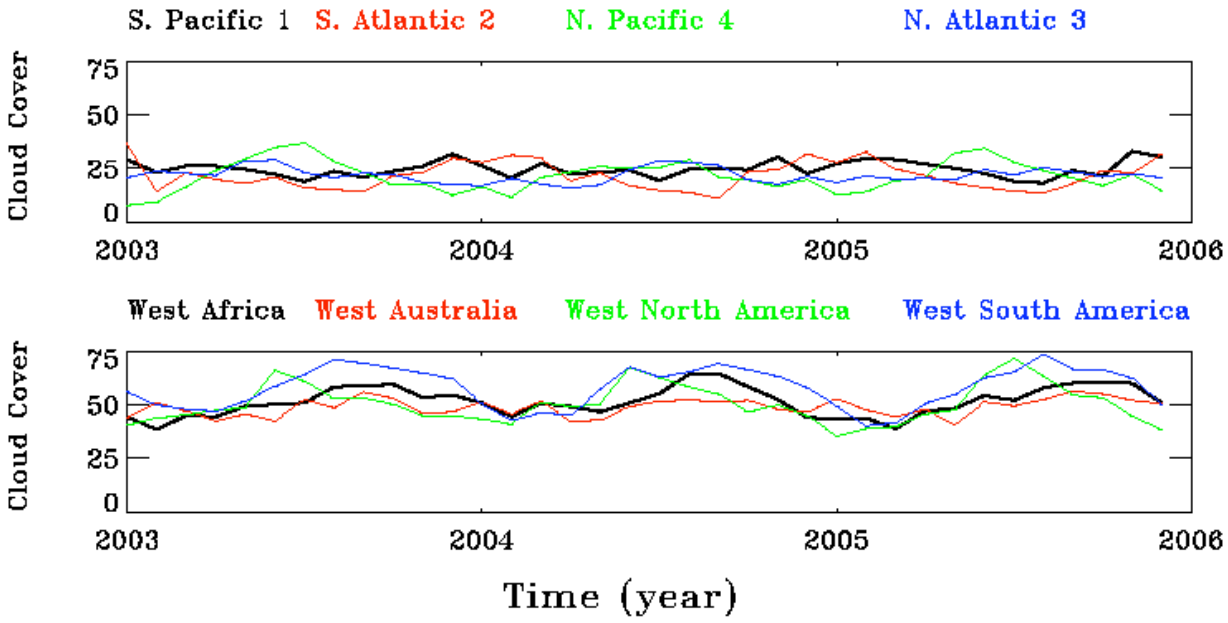

627 Figure 4. Similar as Figure 3, except for selected tropical areas (upper) and combined regions

628 (lower).

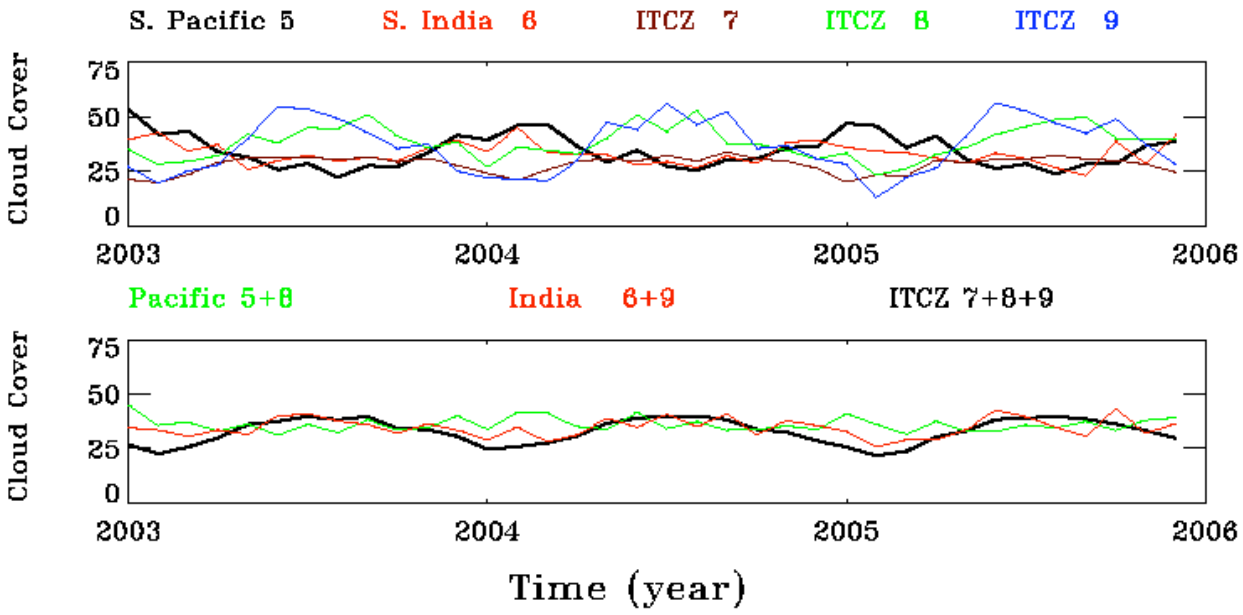

629

630

Figure 5a. Histogram of IWP for high clouds in middle latitude storm tracks during June, July and August (JJA, left) and December, January, and February (DJF, right) for 2003 (black), 2004 (red), and 2005 (green). Means and standard deviations are listed in the left and right columns, respectively, in each plot.

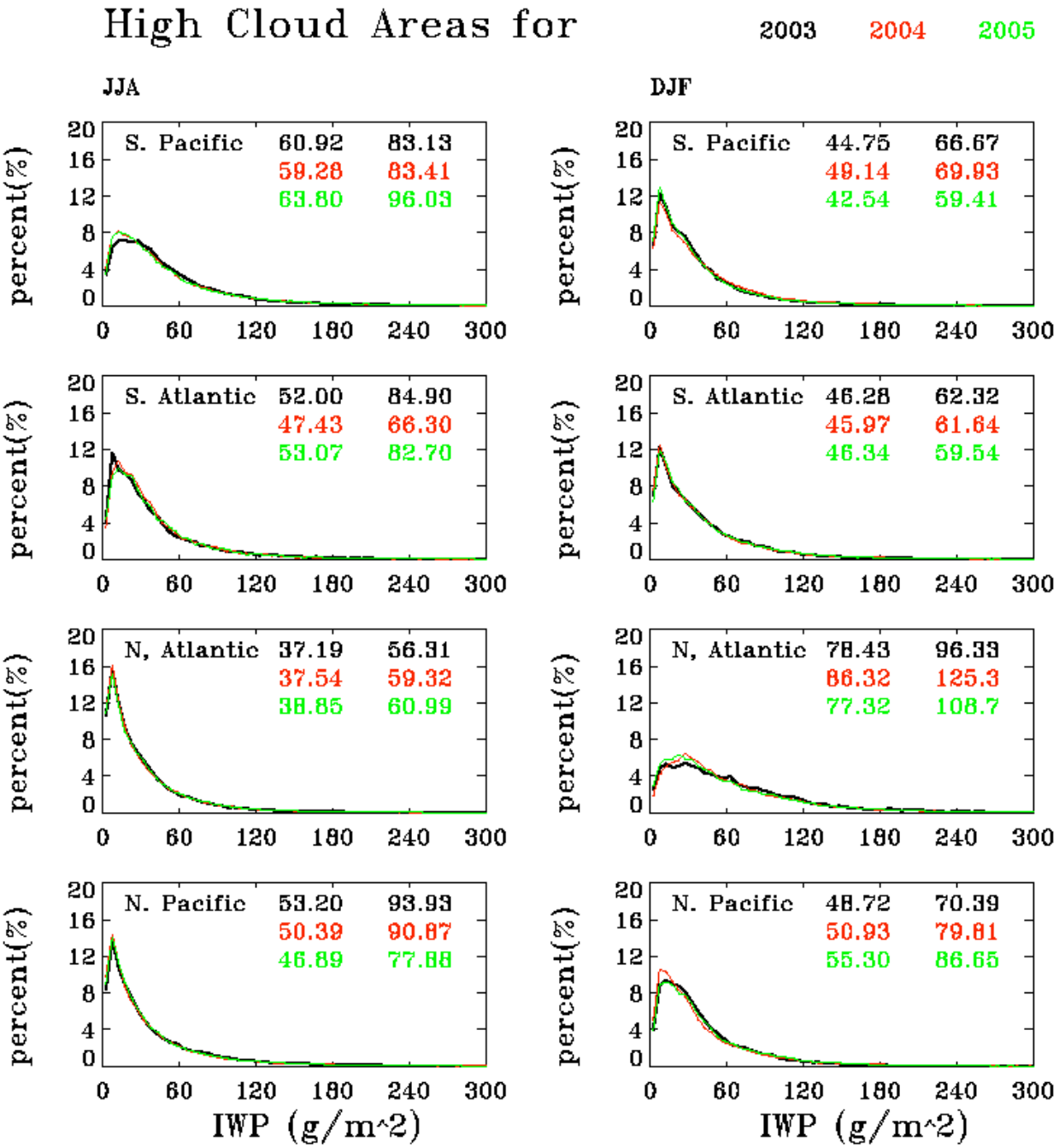

635 Figure. 5b. Same as 5a, except for ITCZ areas.

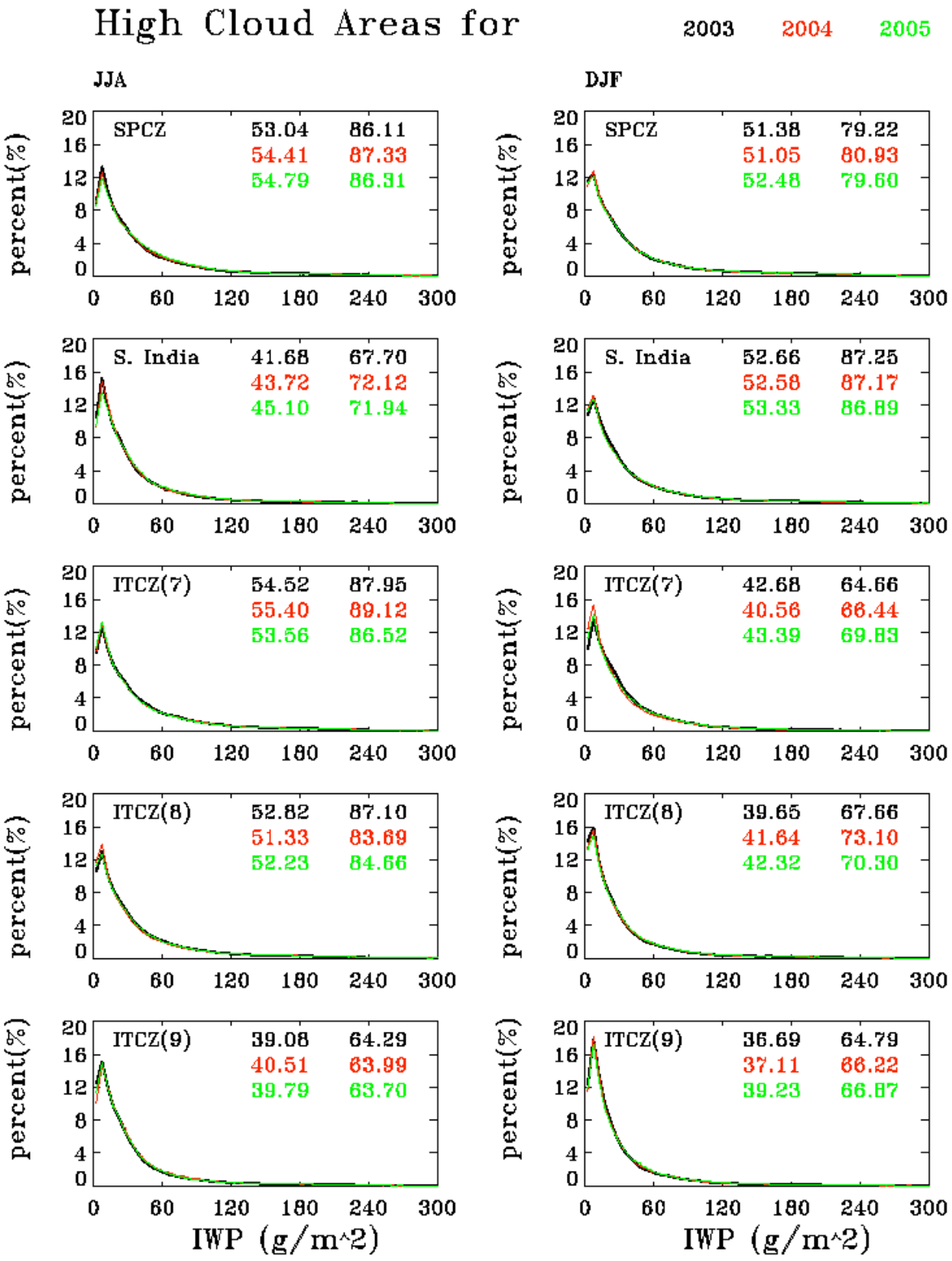

636
637

Figure 6. Histogram of LWP for stratus clouds during June, July and August (JJA, left) and December, January, and February (DJF, right) for 2003 (black), 2004 (red), and 2005 (green).

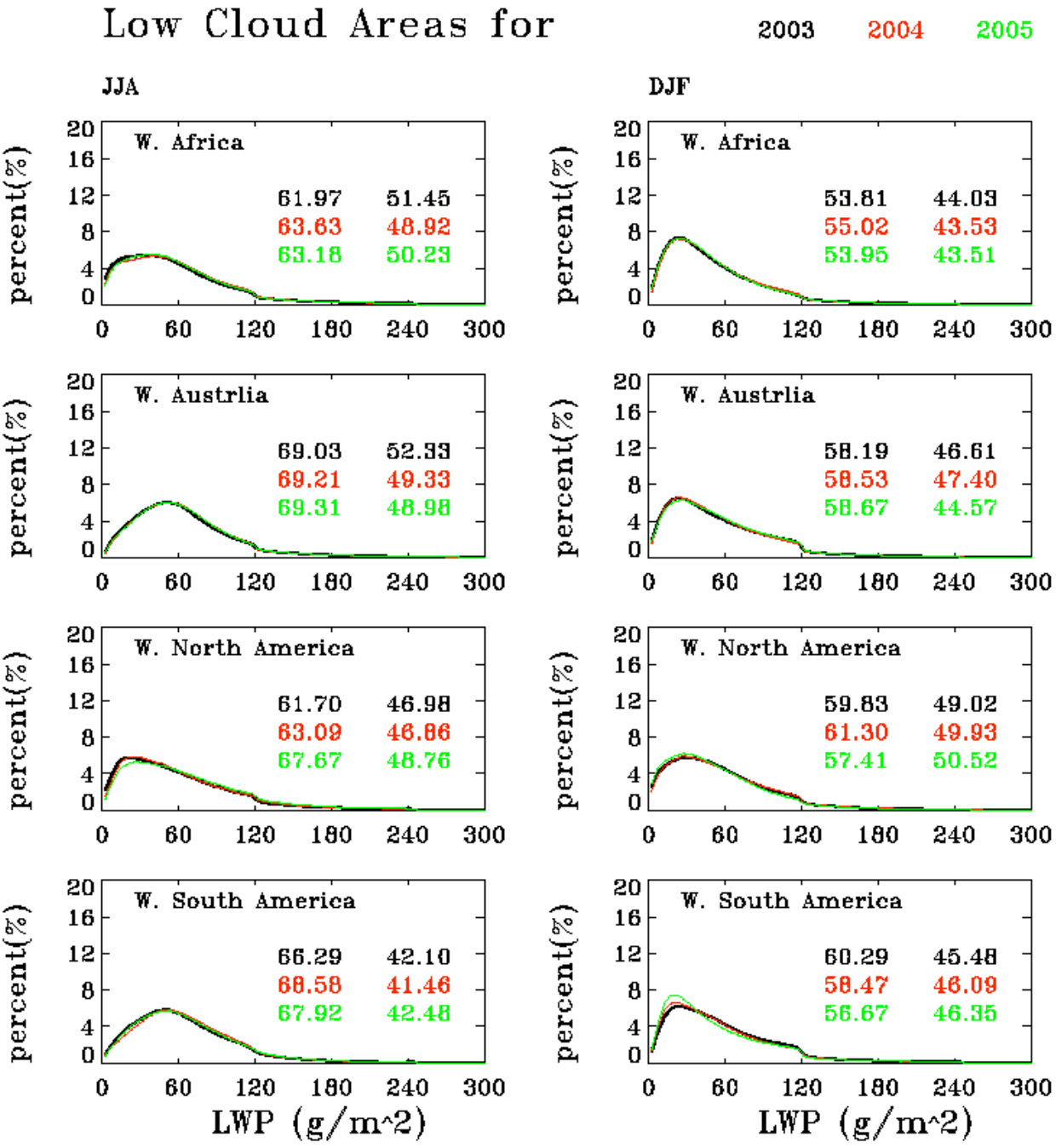

641 Figure 7. Time series of TOA monthly mean net radiation (W/m^2) for clouds in storm track

642 (upper), and stratus (lower) areas.

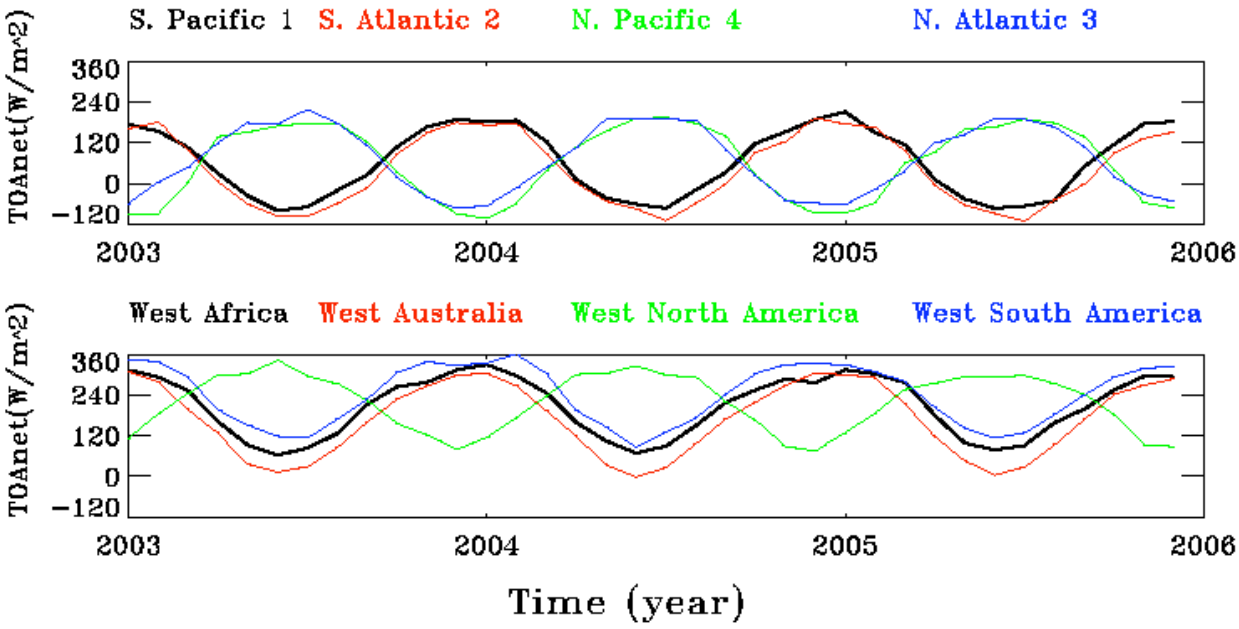

643

644

645

645 Figure 8. Same as Figure 7, except for tropical convergence zones (upper) and their combined

646 high cloud regions (lower).

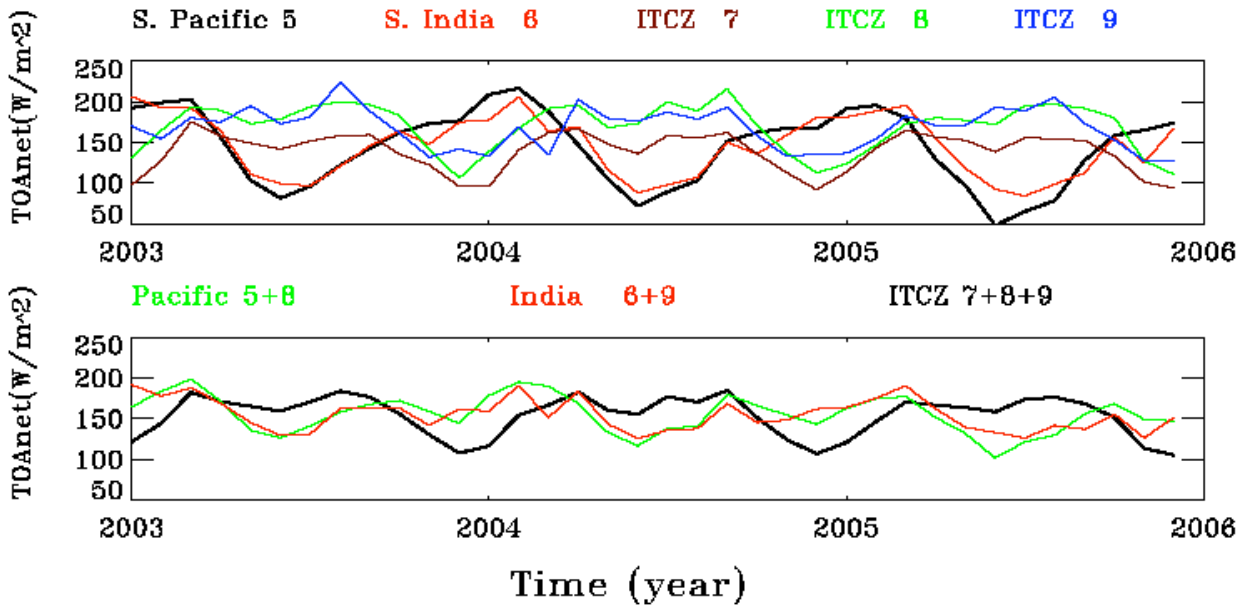

647

648

Figure 9. TOA monthly mean net radiation (W/m^2) for clouds in storm track (upper) and stratus (lower) areas. The Northern Hemisphere radiative fluxes are shifted forward 6 months to obtain the fluxes in the same seasons for all selected areas.

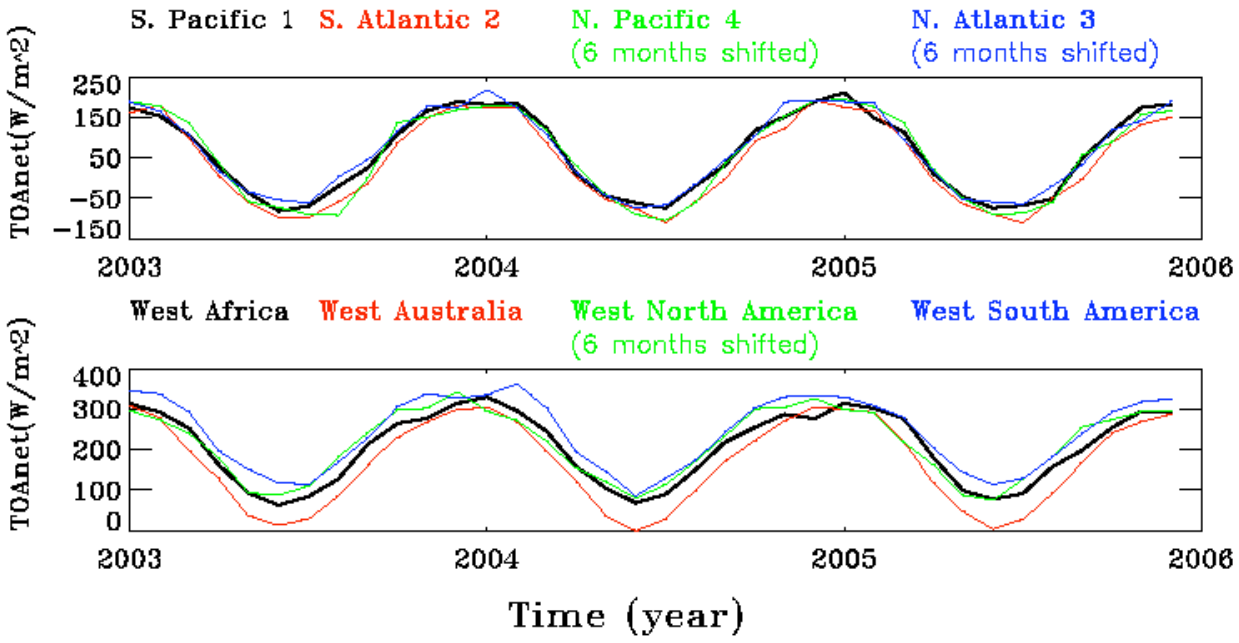

Figure 10. Same as Figure 9, except for surface (SFC) net radiation.

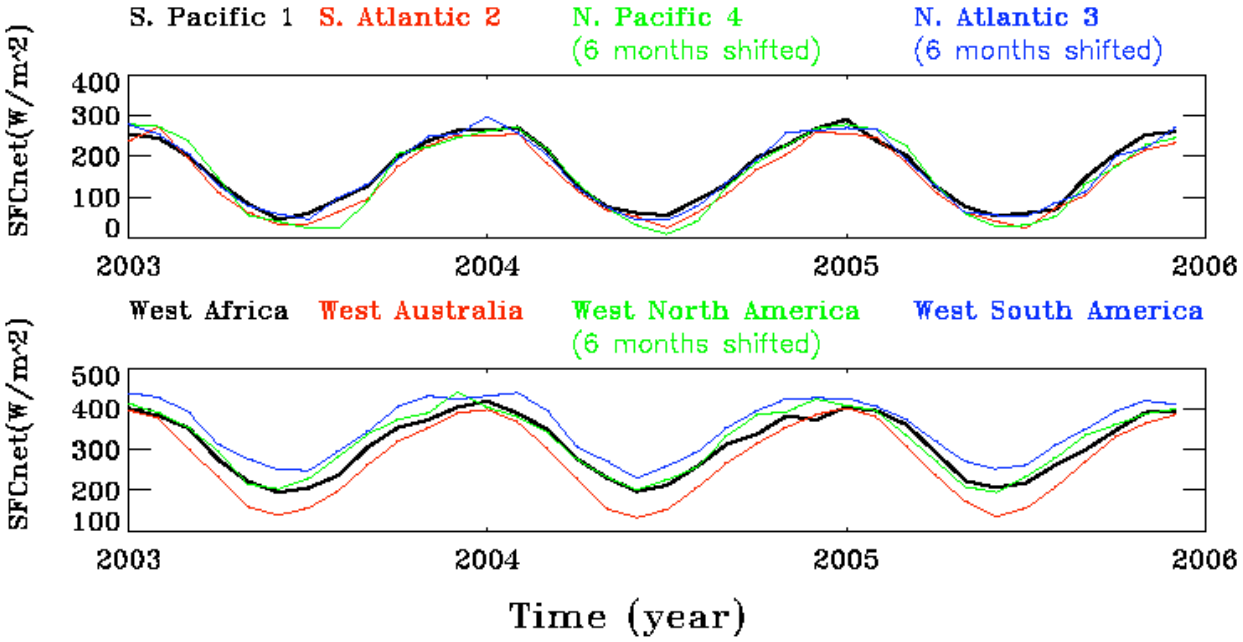

Figure 11. Same as Figure 8, except for surface (SFC) net radiation.

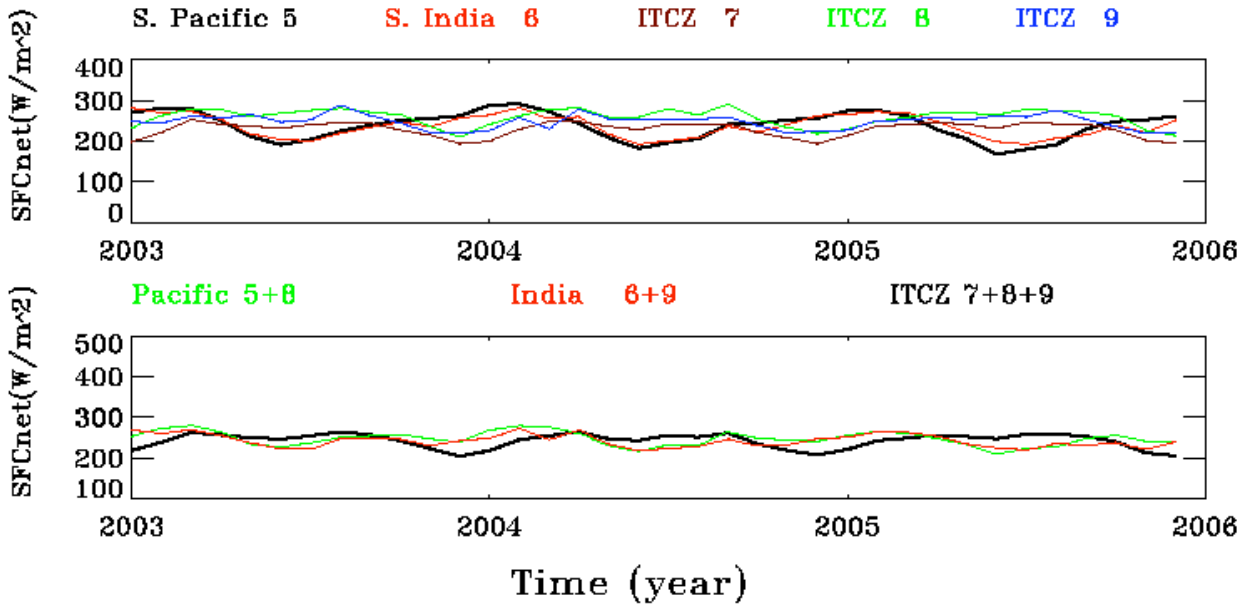

662

663 Figure 12. Time series of monthly mean IWP (mm) for high clouds in selected areas.

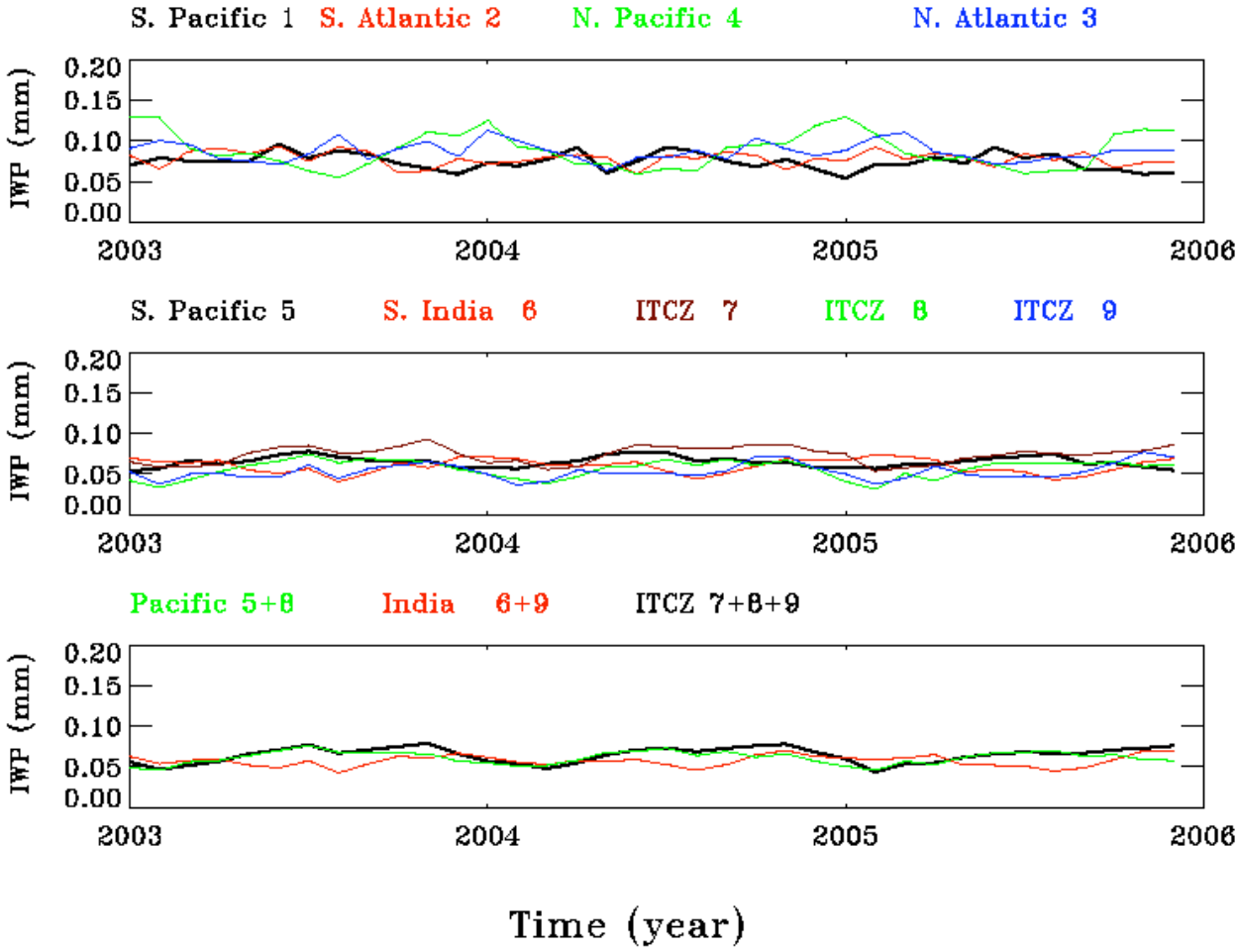

664

665

666

Figure 13. Time series of monthly mean LWP (mm) for low clouds in subtropical solid deck areas.